Int J Adv Manuf Technol (2014) 74:867–878
DOI 10.1007/s00170-014-6041-y

ORIGINAL ARTICLE

Statistical analysis and optimization of processing parameters in high-power direct diode laser cladding

Shuang Liu · Radovan Kovacevic

Received: 9 December 2013 / Accepted: 3 June 2014 / Published online: 14 June 2014
© Springer-Verlag London 2014

Abstract High-power direct diode laser (HPDDL) offers a wide laser beam with a top-hat intensity distribution, making it an ideal tool for large-area cladding. In this study, a systemic study on the HPDDL cladding process was carried out by depositing Fe-based powder on ASTM A36 steel substrate. The effects of input processing parameters (laser power, powder feeding rate, carrier-gas flow rate, and stand-off distance) on the output responses (powder catchment efficiency, clad height, and clad width) were analyzed. The experimental matrix was designed, and a quadratic regression model was developed using a response surface methodology (RSM). Based on the developed model tested by the analysis of variance (ANOVA) method, the relationship between the output responses and the processing parameters were analyzed and discussed. The optimal parameters were identified by the desirability function in order to maximize the powder catchment efficiency, clad height, and clad width.

Keywords High-power direct diode laser (HPDDL) · Response surface methodology (RSM) · Powder catchment efficiency · Clad height · Clad width

1 Introduction

Laser cladding by powder injection, one of the surface modification techniques, has been widely used in the industry to repair or build valuable components and tools. Generally, the powder is fed laterally [1] or coaxially [2] into the molten pool which is generated by a laser beam with a Gaussian intensity distribution. Several clads can be overlapped to cover a large area. The width-to-height aspect ratio is a critical factor that causes the inter-run pores of the overlapped clad and it is desired to be more than 5:1 [3]. However, a Gaussian laser beam tends to produce the clad with a pronounced convex surface that has a lower aspect ratio. In addition, due to the high intensity at the center of a Gaussian laser beam, the dilution of the deposited clad is large [4].

The development of high-power diode lasers (HPDDL) up to 10 kW with a wide rectangular laser spot has great potential in a large-area deposition. Compared with the other high-power lasers (CO_2 or Nd:YAG laser), HPDDL is characterized by a high electricity efficiency, a long lifetime, a good absorption by metals, and low capital and operational costs [5]. HPDDL offers a large rectangular laser spot, allowing the deposition of a wide clad with a flat surface. The top-hat intensity distribution of the diode laser minimizes dilution to only 3 % or even less [6]. With these advantages, many cladding works have been done with HPDDL [7–9]. Well-bonded clads with a small dilution and superior properties were obtained, which indicated the effectiveness and versatility of HPDDL. Very importantly, the multiple tracks overlapped together well to create a very flat surface profile, as shown in Fig. 1.

There exist complex relationships between the input processing parameters such as laser power and powder feeding rate on the deposited results such as powder catchment efficiency and clad geometry. In order to successfully utilize the cladding technique, the processing parameters should be controlled carefully. A number of experiments have been carried out by varying one parameter at a time with a trial-and-error method [2, 10, 11]. However, this method is costly and time consuming, and the obtained results may not be optimal.

The application of statistical methods such as the design of experiments (DoE) is an efficient way to decrease experimental efforts and evaluate the effect of each parameter of interest on the results. For example, a Taguchi design was used by Lee

S. Liu · R. Kovacevic (✉)
Center for Laser-Aided Manufacturing, Southern Methodist University, 3101 Dyer Street, Dallas, TX 75205, USA
e-mail: kovacevi@engr.smu.edu

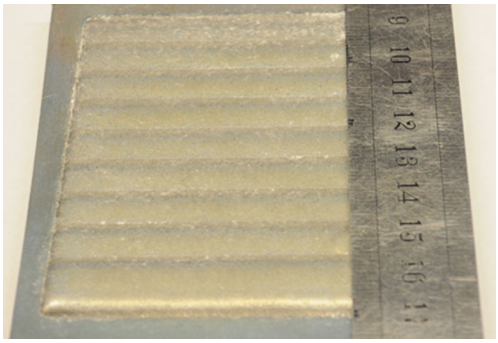

Fig. 1 Multi-track of Fe-based alloy deposited on mild steel plate

[12] to maximize the deposition efficiency. Singh et al. [13] used a full factorial design of experiments in laser-assisted micromachining to optimize the cutting/thrust force and the depth of cut. Graf et al. [14] used a central-composite-design (CCD) method to determine the effects of processing parameters on the clad width and height. Some researchers tried to find out the empirical relations between the clad characteristics and the main processing parameters and to optimize the parameters [15]. Response surface technology (RSM), as one of the main applications of DoE, has been conducted to estimate the unknown mechanism and obtain an optimal response based on a sequence of designed experiments. Manonmani et al. [16] used this method for predicting the effect of laser processing variables on weld geometry. Khan et al. [17] optimized the welding parameters with the quality criteria of maximizing the weld resistance length and shear force, and minimizing the weld width by using RSM. Badkar et al. [18] performed laser transformation hardening for optimizing laser power, scanning speed, and focused position on the hardening width and depth. The application of RSM in the laser cladding process was mainly involved with the optimization of the processing parameters such as laser power, scanning speed, and powder feeding rate. Onmubolu et al. [19] developed a clad wetting-angle model in terms of these parameters and found the optimal parameters to generate the clad with a large wetting angle. Mondal et al. [20] studied the influence of input parameters on the clad height and width. They found that the laser scanning speed and powder feeding rate were the most significant factors. Sun and Hao [21] made a full investigation on clad characteristics including the height, width, width/height ratio, and dilution. They found that the powder feeding rate was the most significant factor. The laser power had a positive effect on clad width. The width/height ratio and dilution increased with an increase in laser power before exceeding the central point and gradually descended when laser power was continuously increased. The powder feeding rate had positive effects on clad height and width whereas negative effects on clad dilution and width/height ratio. Scanning speed had negative effects on clad height, clad width, and dilution.

There is still a lack of application of the statistical analysis method and knowledge of the relations between the cladding results and important parameters in wide-clad deposition. In the HPDDL cladding process, the powder was fed laterally through a wide nozzle into the molten pool by means of a carrier gas. Powder striking the molten pool was completely melted and was used to build up the clad, while powder striking on the solid substrate surface outside the molten pool bounced and was lost or adhered to the hot clad surface. The low powder catchment efficiency is a challenging issue in the process. The characteristics of the clad geometry in determining the clad quality is another critical concern. Therefore, in this work, a study on HPDDL cladding of Fe-based alloy was presented to investigate the effects of the main processing parameters (laser power, powder feeding rate, carrier-gas flow rate, and stand-off distance) on the output results (powder catchment efficiency and clad geometry) and to find out the optimal processing parameters.

2 Experimental design and setup

2.1 Response surface methodology

The cladding parameters and their experimental ranges were determined by the preliminary experiments. Laser power (LP), powder feeding rate (PF), carrier-gas flow rate (CG), and stand-off distance (SD) were selected as optimization variables. The Design Expert version 8 (V8) software was used to code the parameters. CCD is very efficient, providing much information on experiment variable effects and overall experimental error in a minimum number of required runs. A four-factor, three-level CCD matrix was established with 24 axial points and 6 replicated central points. The upper limit of a factor was coded as +1, the lower one was coded as −1, and the middle one was coded as 0. In this study, the measured responses were the powder catchment efficiency, clad height, and clad width. The independent processing parameters with their coded levels are listed Table 1.

Being able to obtain the optimal results, the first step is to develop the relationship between various processing parameters and the corresponding responses. Here, a second-order regression model was used to fit the experimental data, as described in Eq. (1) [22]:

$$y = \beta_0 + \sum_{j=1}^{k} \beta_j x_j + \sum_{j=1}^{k} \beta_{jj} x_j^2 + \sum_{i<j}^{k} \beta_{ij} x_i x_j + \varepsilon \qquad (1)$$

where y is the predict response, β_0 is the intercept coefficient, β_j is the linear coefficient, β_{jj} is the quadratic coefficient, x_j is the processing parameter, k is the number of factors, and ε is

Table 1 Cladding parameters and their levels

Independent variables	Code levels		
	−1	0	1
LP, kW	3	3.5	4
PF, g/min	40	50	60
CG, SCFH	10	15	20
SD, mm	8	10	12

Table 2 Some properties of Fe-based alloy powder and A36 mild steel substrate

Powder	Particle size (μm)	Chemical composition (%)
Fe-based alloy	45–180	1.82 C; 4.5 Mo; 15.9 Ni;0.82 Mn; 28.1 Cr; 1.28 Si; 0.0576 Ni; 0.008 S; Bal. Fe
Substrate	Melting point (°C)	Chemical composition (%)
A36 mild steel	1,480	0.23 C; 0.02 Si; 0.49 Mn; 0.01 S; 0.01 P; 0.01 Ni; 0.03 Cu; Bal. Fe

the associated error. The overall procedure of the parameter optimization is as follows: (a) select design parameters and their limits; (b) develop a design matrix using a central composite design; (c) conduct the experiments; (d) measure the powder catchment efficiency, clad height, and clad width; (e) build the mathematical model to correlate the processing parameters to the results; (f) confirm and validate the model; and (g) select the desirability method and obtain the optimal set of parameters.

2.2 Experimental setup

The experimental setup comprised two powder feeding nozzles installed at the side of the laser head with a tilted angle of 35°, an 8-kW Coherent HPDDL, a 6-axis KUKA robot, and an AT-1200 high-pressure rotary powder feeder, as shown in Fig. 2. The HPDDL was focused into a 12×3 mm^2 rectangular spot. Its divergence angle for the *x*-slow axis and *z*-fast axis was α=23° and β=19°, respectively. In order to protect the lens from the reflection of the light and the ricochet particles, the entire laser head was tilted by 10°. Argon as the shielding gas was supplied to shield the molten pool from oxidation and the lens from the pollution of the fume and ricochet particles. Fe-based alloy powder supplied by Hoganas Company was used during the experiments, and A36 mild steel was selected as the substrate. Some material properties of the powder and substrate are listed in Table 2.

The single-clad experiments were repeated three times at each set of processing parameters. The deposited clads were crosscut, mounted in epoxy resin, and polished to examine the clad geometrical characteristics with respect to the clad height and width. Figure 3 shows the scheme of a typical clad cross section. *H* is the clad height, and *W* is the clad width. The powder catchment efficiency is defined as the ratio between the net clad weight and the fed powder weight. The experimental design matrix and the measured responses are shown in Table 3. Figure 4 presents the clad shape and dimensions of some selected samples.

3 Results and discussion

3.1 Development of the statistical model

Design Expert V8 software was used to develop the model that well described the response factors in regression analysis. The adequacy of the developed relationship was tested using the analysis of variance technique (ANOVA) at the confidence level of 95 %. The insignificant model terms were eliminated by the step-wise regression method.

Tables 4, 5, and 6 show the detailed ANOVA results for the responses (powder catchment efficiency, clad height, and clad width), respectively, where *DF*, SS, MS, *F*, and *p* represent the

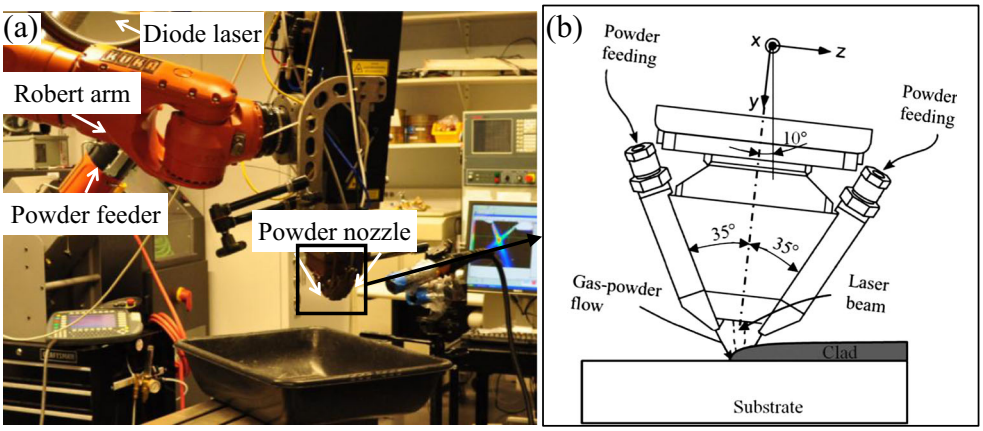

Fig. 2 **a** Experimental setup, **b** laser head installed with powder nozzles [25]

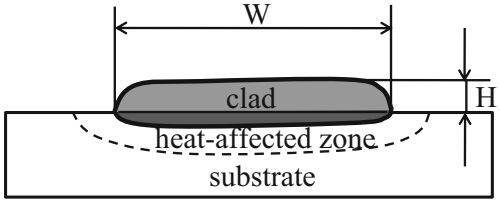

Fig. 3 Scheme of a typical laser clad

degree of freedom, sum of squares, mean of squares, F statistics that is a ratio between group variation and within-group variation, and p value that determines the significance of the test, respectively. The F values of the three models implied the models were significant. The p values of less than 0.01 % indicated the model term was significant. The lack-of-fit F and p values of the models indicated that lack of fits were not significant relative to the pure error. The values of R^2 of 0.829, 0.8938, and 0.907 were close to 1, indicating the high correlation between the experimental and measured data. The "Pred R^2" was in reasonable agreement with the "Adj R^2." "Adeq Precision" detecting the experimental signals-to-noise ratio were 17.491, 22.797, and 18.98, respectively. They were all greater than 4, which indicated an adequate signal.

Table 3 Central composite design of experiments

Exp no.	LP	PF	CG	SD	Catchment efficiency	Clad height	Clad width
1	−1	−1	−1	−1	0.625	1.026	11.785
2	1	−1	−1	−1	0.667	1.713	13.582
3	−1	1	−1	−1	0.608	1.846	11.491
4	1	1	−1	−1	0.627	2.109	13.745
5	−1	−1	1	−1	0.531	1.251	12.127
6	1	−1	1	−1	0.631	1.491	12.455
7	−1	1	1	−1	0.516	2.202	12.173
8	1	1	1	−1	0.584	2.020	13.505
9	−1	−1	−1	1	0.614	1.548	12.280
10	1	−1	−1	1	0.715	1.684	13.713
11	−1	1	−1	1	0.569	2.269	12.116
12	1	1	−1	1	0.609	2.289	13.269
13	−1	−1	1	1	0.284	0.692	12.983
14	1	−1	1	1	0.487	1.116	12.396
15	−1	1	1	1	0.356	1.173	13.154
16	1	1	1	1	0.430	1.385	13.501
17	−1	0	0	0	0.563	1.554	12.450
18	1	0	0	0	0.641	1.738	13.430
19	0	−1	0	0	0.649	1.684	13.080
20	0	1	0	0	0.588	2.043	13.136
21	0	0	−1	0	0.640	1.842	12.999
22	0	0	1	0	0.514	1.500	12.029
23	0	0	0	−1	0.525	2.028	12.416
24	0	0	0	1	0.444	1.660	13.265
25	0	0	0	0	0.641	1.678	12.530
26	0	0	0	0	0.654	1.766	12.500
27	0	0	0	0	0.586	1.589	12.940
28	0	0	0	0	0.707	1.850	12.63
29	0	0	0	0	0.680	1.706	12.58
30	0	0	0	0	0.603	1.498	12.53

Seen from Table 4, the analysis of variable result for the powder catchment efficiency shows that the carrier gas (CG) had the most significant effect; the laser power (LP) as well as the first (SD) and second order [$(SD)^2$] of the stand-off distance had less effect; the interaction of carrier gas and stand-off distance [(CG)(SD)] had the least effect. For the clad height model, the results in Table 5 show that the powder feeding rate (PF), carrier-gas flow rate (CG), and interaction of the carrier gas and stand-off distance [(CG)(SD)] were the most associated with the clad height; the laser power (LP) and stand-off distance (SD) had less effect; the second order of laser power [$(LP)^2$] as well as the interaction of the laser power and powder feeding rate [(LP)(PF)] had the least effect. In the clad width model, the analysis of variance results in Table 6 show that the laser power (LP) was the most significant term. The stand-off distance (SD), carrier gas (CG), interaction of the laser power and stand-off distance [(LP)(SD)], and interaction of the laser power and carrier gas [(LP)(CG)] had less effect. The powder feeding rate (PF) had the least effect.

The final models for the corresponding responses in terms of coded factors are shown in Eqs. (2), (3), and (4).

$$\text{Powder catchment efficiency} = 0.62 + 0.042(\text{LP}) - 0.074(\text{CG}) - 0.044(\text{SD}) - 0.042(\text{CG})(\text{SD}) - 0.076(\text{SD})^2 \quad (2)$$

$$\text{Clad height} = 1.74 + 0.11(\text{LP}) + 0.29(\text{PF}) - 0.19(\text{CG}) - 0.1(\text{SD}) - 0.073(\text{LP})(\text{PF}) - 0.23(\text{CG})(\text{SD}) - 0.12(\text{LP})^2 \quad (3)$$

$$\text{Clad wdith} = 12.75 + 0.65(\text{LP}) - 0.057(\text{PF}) + 0.16(\text{CG}) + 0.19(\text{SD}) - 0.16(\text{LP})(\text{CG}) - 0.2(\text{LP})(\text{SD}) + 0.2(PF)^2 \quad (4)$$

and the final models in terms of actual factors are shown below:

$$\text{Powder catchment efficiency} = -1.7546 + 0.0832(\text{LP}) + 0.0272(\text{CG}) + 0.42(\text{SD}) - 0.0042(\text{CG})(\text{SD}) - 0.019(\text{SD})^2 \quad (5)$$

$$\text{Clad height} = -11.269 + 4.314(\text{LP}) + 0.08(\text{PF}) + 0.192(\text{CG}) + 0.294(\text{SD}) - 0.0147(\text{LP})(\text{PF}) - 0.023(\text{CG})(\text{SD}) - 0.48(\text{LP})^2 \quad (6)$$

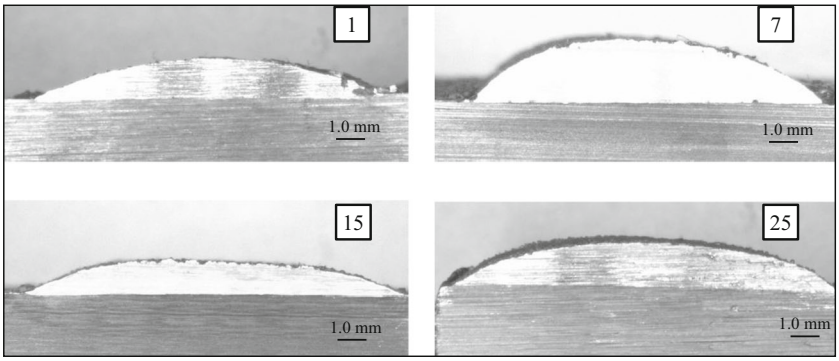

Fig. 4 Cross section of the selected clad (*the number* on each graph indicates the experiment number in Table 3)

Table 4 ANOVA for powder catchment efficiency

Source	SS	*DF*	MS	*F*	*p*	Prob>*F*
Model	0.23	5	0.047	19.04	<0.0001	Significant
LP	0.031	1	0.031	20.47	0.0006	
CG	0.098	1	0.098	54.62	<0.0001	
SD	0.035	1	0.035	17.42	0.0003	
(CG)(SD)	0.028	1	0.028	21.6	0.0010	
$(SD)^2$	0.041	1	0.041	17.31	0.0001	
Residual	0.048	24	0.00202			
Lack of fit	0.038	19	0.002	0.96	0.5799	Not significant
Pure error	0.010	5	0.00209			
Cor total	0.28	29				

R^2 =0.829
Adj R^2 =0.793
Pred R^2 =0.736
Adeq precision=17.491

$$\text{Clad wdith} = 1.683 + 4.283(\text{LP}) - 0.209(\text{PF}) + 0.25(\text{CG}) + 0.811(\text{SD}) - 0.0625(\text{LP})(\text{CG}) - 0.204(\text{LP})(\text{SD}) + 0.002(PF)^2 \quad (7)$$

3.2 Validation of the developed model

Generally, it is necessary to check the developed model before investigation or optimization of the responses. The normal probability plot of the studentized residuals was one of the most important diagnostics, as shown in Fig. 5. It can be seen that the normality assumption was satisfied as the residual plot approximated along a straight line. Figure 6 further confirms the predicted model, where the calculated responses according to Eqs. (5), (6), and (7) were plotted as the functions of the measured data. It was demonstrated that the predicted values agreed well with measured results.

Table 5 ANOVA for clad height

Source	SS	*DF*	MS	*F*	*p*	Prob>*F*
Model	3.6	7	0.51	26.45	<0.0001	Significant
LP	0.22	1	0.22	11.26	0.0029	
PF	1.46	1	1.46	75.29	<0.0001	
CG	0.68	1	0.68	34.95	<0.0001	
SD	0.19	1	0.19	10	0.0045	
(LP)(PF)	0.086	1	0.086	4.43	0.0469	
(CG)(SD)	0.85	1	0.85	43.9	<0.0001	
$(LP)^2$	0.1	1	0.1	5.34	0.0306	
Residual	0.43	22	0.019			
Lack of fit	0.35	17	0.021	1.31	0.4116	Not significant
Pure error	0.078	5	0.016			
Cor total	4.02	29				

R^2 =0.8938
Adj. R^2 =0.86
Pred. R^2 =0.7782
Adeq precision=22.797

Table 6 ANOVA for clad width

Source	SS	*DF*	MS	*F*	*p*	Prob>*F*
Model	10.2	7	1.46	30.56	<0.0001	Significant
LP	7.68	1	7.68	160.92	<0.0001	
PF	0.059	1	0.059	1.23	0.2788	
CG	0.43	1	0.43	9.12	0.0063	
SD	0.68	1	0.68	14.27	0.001	
(LP)(CG)	0.39	1	0.39	8.18	0.0091	
(LP)(SD)	0.67	1	0.67	13.95	0.0011	
$(PF)^2$	0.3	1	0.3	6.21	0.0207	
Residual	1.05	22	0.048			
Lack of fit	0.91	17	0.054	2	0.2283	Not significant
Pure error	0.13	5	0.027			
Cor total	11.25	29				

R^2 =0.907
Adj. R^2 =0.877
Pred R^2 =0.837
Adeq. Precision=18.98

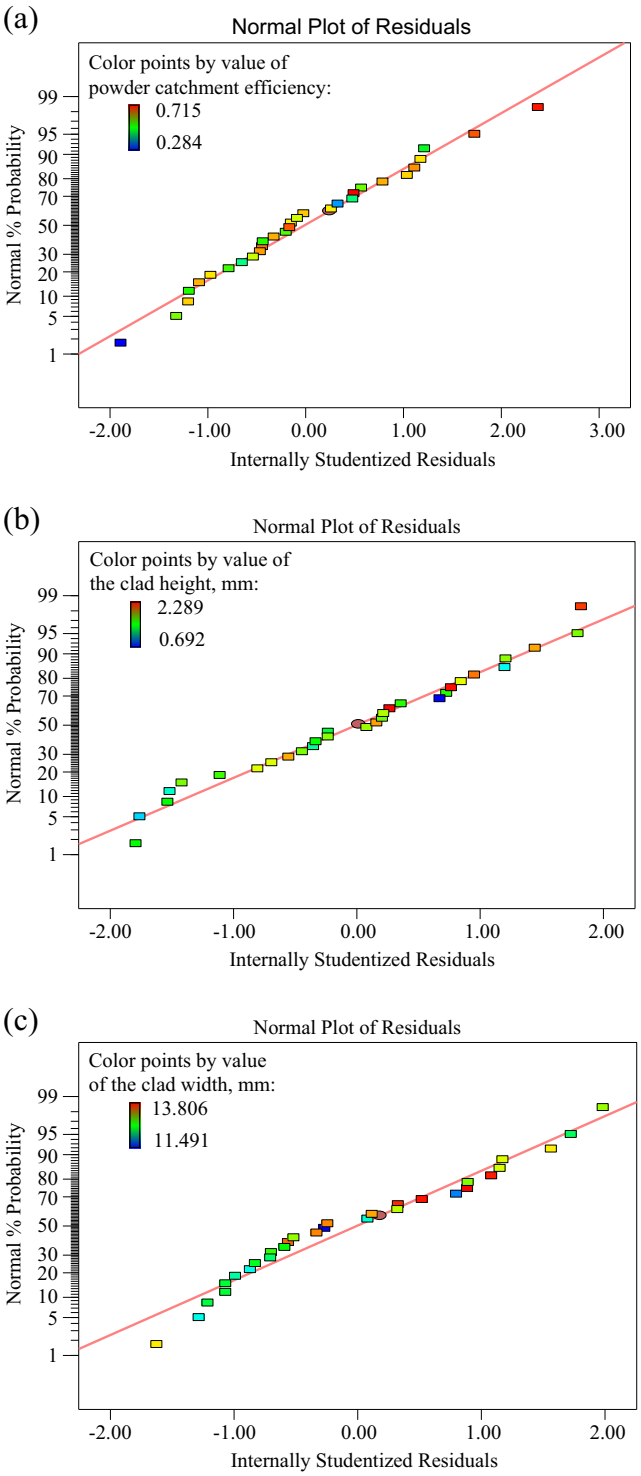

Fig. 5 Normal probability plot of residuals for **a** powder catchment efficiency, **b** clad height, and **c** clad width

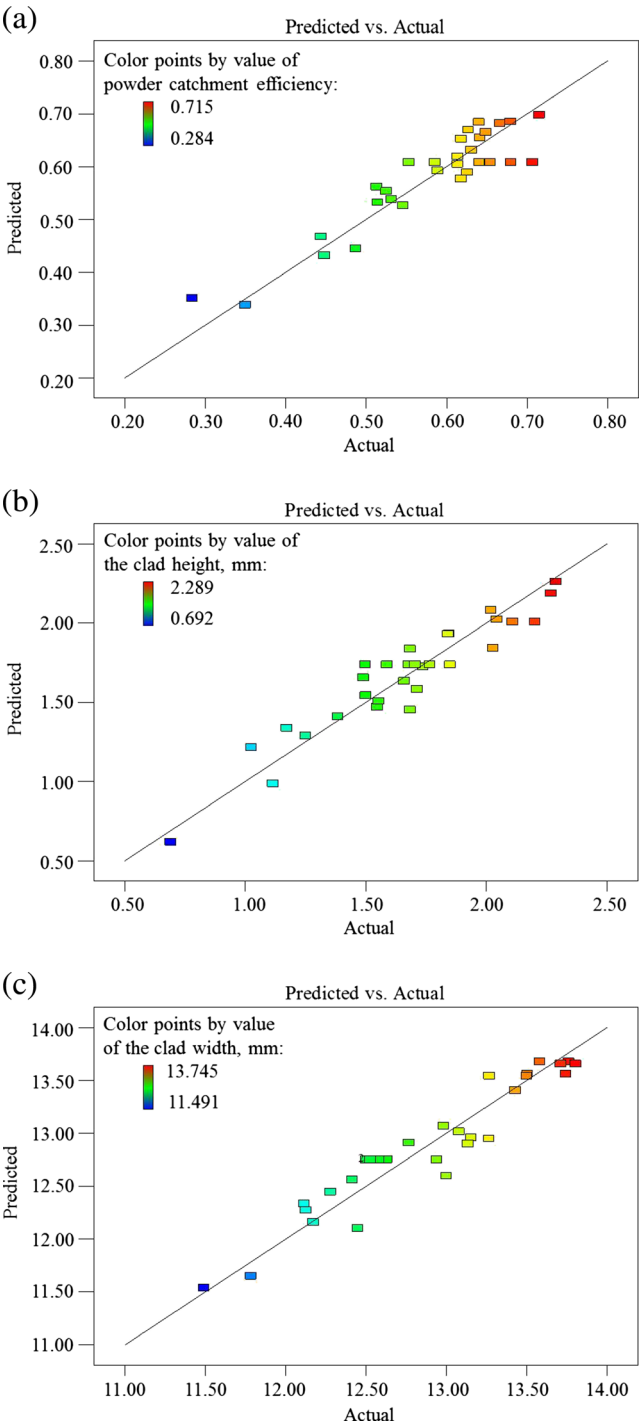

Fig. 6 Predicted vs. measured **a** powder catchment efficiency, **b** clad height, and **c** clad width

Besides, three confirming experiments were carried out with the new cladding conditions within the range defined earlier. For the actual responses, the value was obtained by averaging three measured results. Table 7 summarizes the experimental conditions, the actual responses, the predicted values, and the percentage of errors. The results demonstrated that the developed models were quite accurate for prediction.

3.3 Effects of cladding process parameters

The effects of processing parameters on powder catchment efficiency, clad height, and clad width were evaluated in terms

Table 7 Confirmation experiments

Exp. no.	LP, kW	PF, g/min	CG, SCFH	SD, mm		Powder catchment efficiency	Clad height, mm	Clad width, mm
1	3.25	45	12.5	9	Actual	0.653	1.594	12.4
					Predicted	0.6243	1.5901	12.1657
					Error %	4.395	0.243	1.890
2	3.75	55	17.5	11	Actual	0.5459	1.701	12.85
					Predicted	0.586	1.6931	13.0787
					Error %	−7.346	0.463	−1.780

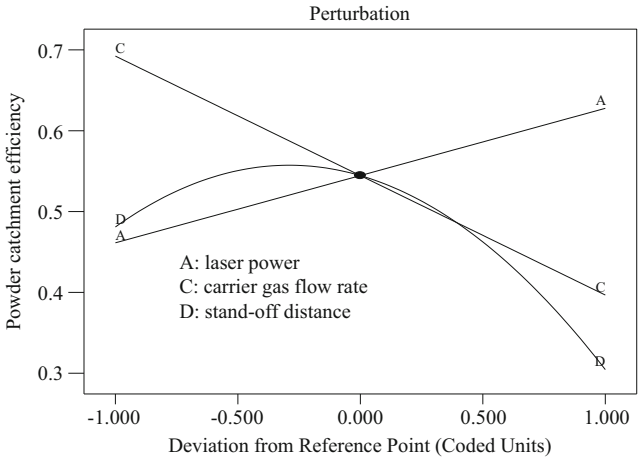

Fig. 7 Perturbation plot illustrating the influences of the input variables on powder catchment efficiency

of perturbation and 3D surface plots. The perturbation plots were used to present the effect of all the parameters with respect to a center point of the design space. The 3D surface plot was used to investigate the effect of some significant interactive terms.

3.3.1 Powder catchment efficiency

Figure 7 presents the perturbation plots to show the effect of each processing parameter on the powder catchment efficiency. It could be seen that the laser power had a positive effect on the powder catchment efficiency, while the carrier-gas flow rate had a negative effect. Increasing the stand-off distance until it reached the center value improved the powder catchment efficiency. Then, the powder catchment efficiency descended as the stand-off distance was continuously increased. A higher laser power generated a larger molten pool with a higher temperature. More particles were captured and melted to form the clad. The powder particles that were fed with a lower carrier-gas flow rate traveled slower in flight and had a longer interaction time with the laser beam. They were more likely melted and clung to the clad surface. As seen in Fig. 8, at a low carrier gas, some of the particles which did

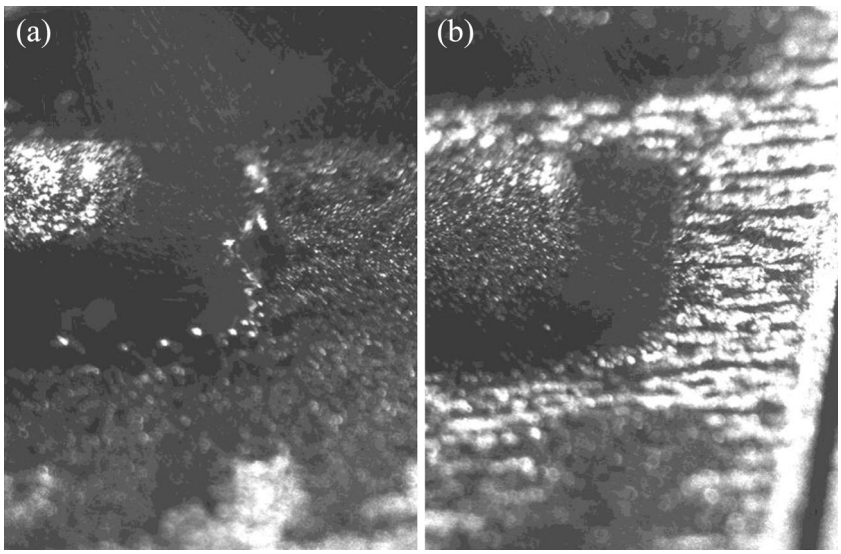

Fig. 8 CCD images of the molten pool at the carrier-gas flow rate of **a** 10 SCFH and **b** 20 SCFH

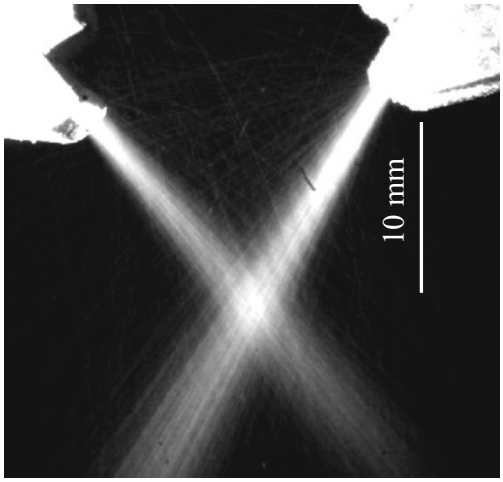

Fig. 9 Powder flow image

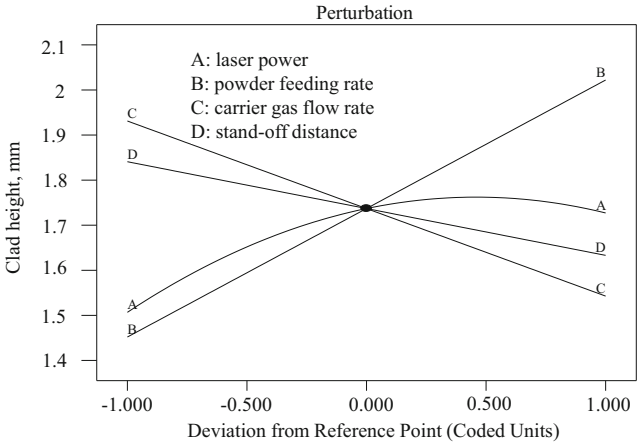

Fig. 11 Perturbation plot illustrating the influences of the input variables on clad height

not enter the molten pool remained on the substrate surface. When the substrate was moving, the particles in front of the molten pool were melted and contributed to the deposition volume of the clad. At a high carrier-gas flow rate, the particles with a high traveling speed were bounced off or blown away by the gas flow. Moreover, too high carrier-gas flow rate affected the convection of the molten pool and might cause the irregular surface of the deposited clad [23]. Figure 9 shows that the two powder flows converged at around the distance of 10 mm where a maximum powder concentration was obtained. The substrate placed away from the intersection position would decrease the powder catchment efficiency.

The ANOVA summary shown in Table 4 indicated that the interactive model term of carrier-gas flow rate and stand-off distance was significant. Figure 10a and b shows a 3D surface plot and a contour graph illustrating the effect of carrier-gas flow rate and stand-off distance on the powder catchment efficiency. It shows that at a stand-off distance of 10 mm, a lower carrier-gas flow rate could provide a higher powder catchment efficiency. A high stand-off distance combined with a high carrier-gas flow rate would result in a much lower powder catchment efficiency.

3.3.2 Clad height

Figure 11 presents the perturbation plots to show the effects of all parameters on the clad height. It could be seen that the clad height increased with an increase in powder feeding rate. At a higher powder feeding rate, more particles were injected into the molten pool, contributing to the height of the clad. The carrier-gas flow rate and stand-off distance had negative effects on the clad height. Moreover, the effect of carrier gas was more significant than the stand-off distance. An increase in the carrier-gas flow rate would decrease the powder catchment efficiency, resulting in a lower clad height. The farther the substrate was placed from the nozzle, the worse convergence of the powder stream had, and less the portion of powder was deposited. It was also observed that the clad height was rapidly increased with an increase in laser power before approaching the center point of the design space and then

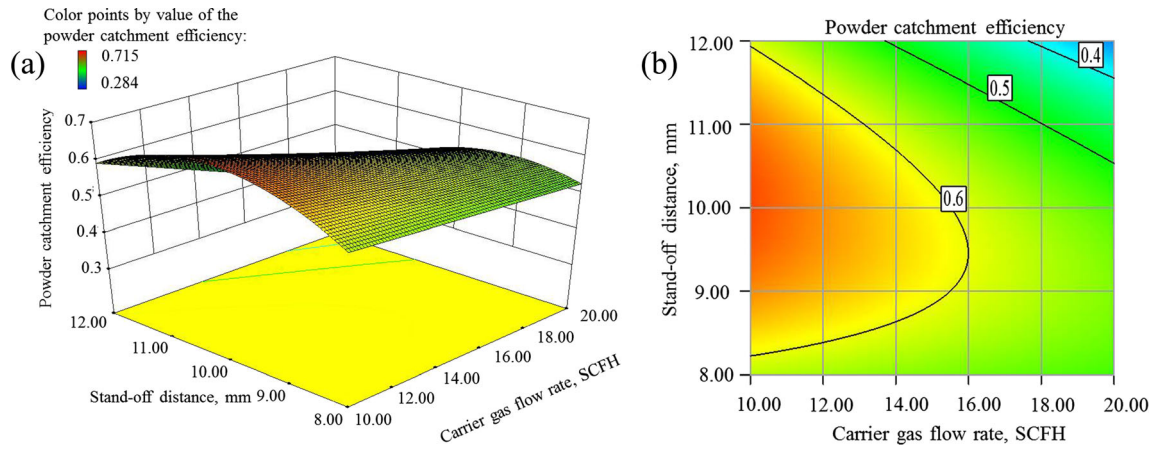

Fig. 10 **a** 3D surface plot and **b** contour graph of interaction effect of carrier-gas flow rate and stand-off distance on powder catchment efficiency

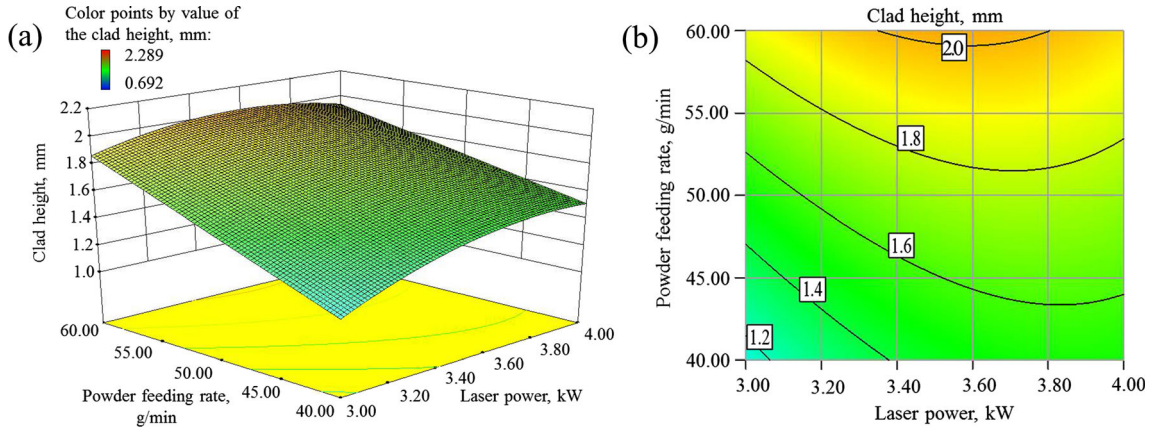

Fig. 12 **a** 3D surface plot and **b** contour graph of interaction effect of laser power and powder feeding rate on clad height

descended gradually. An increase of laser power enlarged the molten pool size that would melt more particles, contributing to the higher clad. While the laser power surpassed the central point, the high temperature in the molten pool decreased the viscosity of the liquid metal. As a result, the material spread out and the clad height decreased.

In the ANOVA in Table 5 shown above, the interactive model term of laser power and powder feeding rate was significant. Figure 12a and b presents a 3D surface plot and a contour graph illustrating the effect of the laser power and powder feeding rate on the clad height. It shows that a large powder feeding rate combined with a high laser power would produce a high clad.

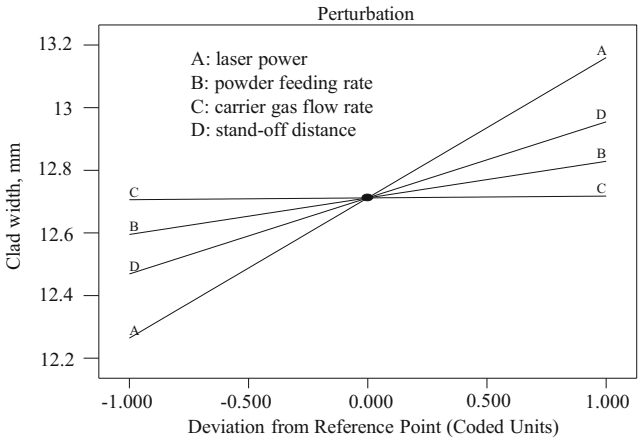

Fig. 13 Perturbation plot illustrating the influences of the input variables on clad width

3.3.3 Clad width

Figure 13 shows the perturbation plots to illustrate the effects of all parameters on the clad width. It could be seen that the clad width increased with an increase in laser power, powder feeding rate, and stand-off distance. Obviously, the high laser power generated a larger molten pool. At a higher powder feeding rate, more particles were injected into the molten pool and the molten pool overflowed. As a result, the clad width was increased. The effect of the stand-off distance on the clad width was related to the convergence of the powder flow and

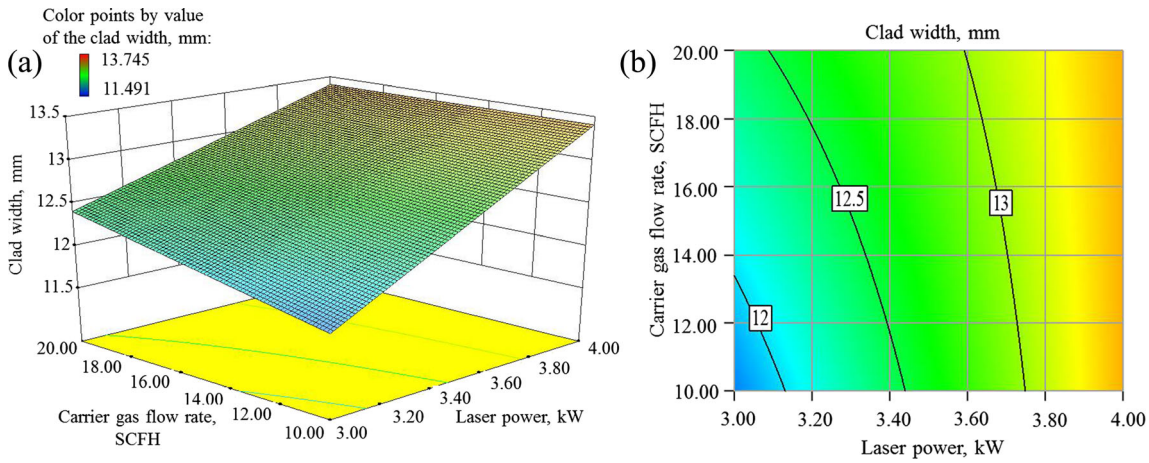

Fig. 14 **a** 3D surface plot and **b** contour graph of interaction effect of laser power and carrier-gas flow rate

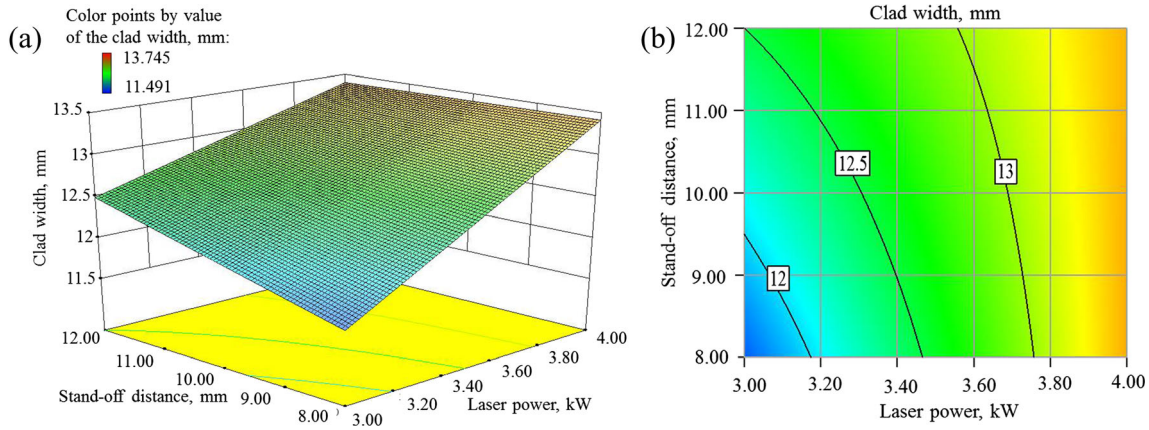

Fig. 15 **a** 3D surface plot and **b** contour graph of interaction effect of laser power and stand-off distance on clad width

the interaction between the powder flow and the laser beam. The clad width was almost kept constant at different carrier-gas flow rates.

In the ANOVA in Table 6 shown above, the interactive model terms of laser power and carrier gas, as well as laser power and stand-off distance were significant. Figure 14a and b presents a 3D surface plot and a contour graph illustrating the effect of laser power and carrier gas on the clad width. It shows that a high laser power combined with a large carrier-gas flow rate would produce a wide clad. Figure 15a and b presents a 3D surface plot and a contour graph illustrating the effect of laser power and stand-off distance on the clad width. It shows that a high laser power combined with a large stand-off distance would increase the clad width.

Table 8 Optimization criteria used in this study

Parameter or response	Criteria	Limits		Importance
		Lower	Upper	
LP, kW	Is in range	3	4	3
PF, g/min	Is in range	40	60	3
CG, SCFH	Is in range	10	20	3
SD, mm	Is in range	8	12	3
Powder catchment efficiency	Maximize	0.284	0.715	5
Clad height, mm	Maximize	0.692	2.289	5
Clad width, mm	Maximize	11.491	13.745	3

3.4 Optimization and confirmation

The desirability function approach is one of the most widely used methods in industry for the optimization of processing parameters with multiple responses [24]. The general approach of the desirability function is to transfer each response into a desirability function D bounded between 0 and 1. In the current study, a maximum requirement is set for powder catchment efficiency, clad height, and clad width. Hence, the desirability function can be defined as follows [24]:

$$D(f(x_i)) = \begin{cases} 0 & \text{if } f(x_i) \le f_{\min} \\ \left(\dfrac{f - f_{\min}}{f_{\max} - f_{\min}}\right)^r, & \text{if } f_{\min} \le f(x_i) \le f_{\max} \\ 1 & \text{if } f(x_i) \ge f_{\max} \end{cases} \quad (8)$$

Table 9 Optimal solutions as obtained by Design Expert V8 based on the criteria

Number	LP, kW	PF, g/min	CG, SCFH	SD, mm	Powder catchment efficiency	Clad height, mm	Clad width, mm	Desirability
1	4	59.99	10	11.06	0.715	2.200	13.547	0.952
2	4	60	10	11.1	0.714	2.202	13.548	0.951
3	3.99	60	10	11.04	0.715	2.203	13.533	0.951
4	4	60	10	10.95	0.720	2.193	13.548	0.950
5	3.97	60	10	11.01	0.715	2.207	13.511	0.950
6	4	60	10.12	11.01	0.715	2.190	13.548	0.949
7	3.98	60	10	10.91	0.719	2.199	13.517	0.948
8	4	60	10.23	10.95	0.715	2.180	13.548	0.947
9	4	59.33	10	11.06	0.715	2.186	13.525	0.946
10	3.94	59.97	10	10.93	0.715	2.215	13.459	0.946

Fig. 16 Cross section of the clad deposited under the optimal operative conditions

where f_{min} is the lower value, f_{max} is the upper value, and r is a weight to indicate the shape of the desirability function. Desirability of the response increases when value of the response approaches the desired target. To determine the optimal experimental condition for HPDDL cladding, Design Expert V8 was utilized for the optimization operation. Table 8 summarized the optimization criteria of the multiple responses.

The most desirable experimental conditions were listed in Table 9. It can be seen that the ranges of the most desirable processing parameters are laser power from 3.94 to 4 kW, powder feeding rate from 59.33 to 60 g/min, carrier-gas flow rate from 10 to 10.23 standard cubic feet per minute (SCFH), and stand-off distance from 10.91 to 11.1 mm. In order to validate the optimal operative conditions, the experiment was performed at the parameters of LP=4 kW, PF=60 g/min, CG=10 SCFH, and SD=11.1 mm. The cross section of the clad was shown in Fig. 16, and the results were listed in Table 10. It proves that using the optimal parameters the clad with desirable requirements could be obtained. Moreover, the measured results were found in good agreement with the predicted values.

4 Conclusions

The current study mainly involves the statistical analysis and optimization of processing parameters in laser cladding of Fe-based powder using HPDDL. Several conclusions can be drawn as follows:

(1) The empirical relationships were developed to predict the powder catchment efficiency as well as the clad height and width using RSM. The predicted values agreed well with the experimental results.

Table 10 Difference between the actual and predicted results under optimal operative conditions

Source	Powder catchment efficiency	Clad height, mm	Clad width, mm
Actual	0.679	2.354	13.521
Predicted	0.714	2.202	13.548
Error %	−5.15	6.46	−0.02

(2) According to the results of ANOVA tables, the carrier-gas flow rate had the most significant effect on the powder catchment efficiency. The powder feeding rate, carrier-gas flow rate, and interaction of the carrier gas and stand-off distance were the most significant factors affecting the clad height. The laser power was the most effective factor affecting the clad width.

(3) The desirability optimization results show that the processing parameters of laser power from 3.94 to 4 kW, powder feeding rate from 59.33 to 60 g/min, carrier-gas flow rate from 10 to 10.23 SCFH, and stand-off distance at 10.91 to 11.1 mm were the optimal setting to obtain the high powder catchment efficiency, and large clad height and width. The obtained results could be of a great interest to the uses of high-power laser cladding process.

Acknowledgments The authors also would like to thank Fanrong Kong and Andrew Socha in the Center for Laser-aided Manufacturing for the help in the execution of the experiments. The work was financially supported by the NSF Grant no. IIP-1034652.

References

1. Gong XY, Zhang YZ, Liu MK (2013) Powder transport model for laser cladding by lateral powder feeding: I. Powder flow field with cylindrical distribution. Inter Adv Manuf Technol 67:2501–2509
2. Oliveira U, Ocelik V, Hosson J (2005) Analysis of coaxial laser cladding processing conditions. Surf Coat Technol 197:127–136
3. Yellup JM (1995) Laser cladding using the powder blowing technique. Surf Coat Technol 71:121–128
4. Schoeffel KC, Shin YC (2007) Laser cladding of two hardfacing alloys onto cylindrical low alloy steel substrates with a high power direct diode laser. In: Proceedings of the International Manufacturing Science and Engineering Conference (MSEC), Atlanta, USA.
5. Li L (2000) The advances and characteristics of high-power diode laser materials process. Opt Las Eng 34:231–253
6. Coherent Inc, Cladding with high power diode lasers, http://www.coherent.com/downloads/CladdingWithHPDDL_WhitepaperFinal.pdf.
7. Nowotny S, Richter A, Beyer E (1998) Laser cladding using high-power diode lasers. In: International Congress on Application of Lasers & Electro-Optics (ICALEO), Orlando, USA, pp. 68–74.
8. Uenishi K, Ogata Y, Iwatani S, Adachi A, Sato T, Kobayashi K (2007) Laser cladding of Fe-Cu based alloys on aluminum. Solid State Phenom 127:331–336
9. Santhanakrishnan S, Kong F, Kovacevic R (2011) An experimentally based thermo-kinetic hardening model for high power direct diode laser cladding. J Mater Process Technol 211:1247–1259
10. Chryssolouris G, Zannis S, Tsirbas K, Lalas C (2002) An experimental investigation of laser cladding. CIRP Ann-Manuf Technol 51(1): 145–148
11. Song JL, Li YT, Deng QL, Hu DJ (2006) Experimental study of laser cladding forming iron-based alloys. In: International Technology and Innovation Conference (ITIC), London, UK.
12. Lee HK (2008) Effects of the cladding parameters on the deposition efficiency in pulsed Nd: YAG laser cladding. J Mater Process Technol 202:321–327

13. Singh RK, Joseph VR, Melkote SN (2011) A statistical approach to the optimization of a laser-assisted micromachining process. Int J Adv Manuf Technol 53:221–230
14. Graf B, Ammer S, Gumenyuk A, Rethmeier M (2013) Design of experiments for laser metal deposition in maintenance, repair and overhaul applications. Procedia CIRP 11:245–248
15. Palani PK, Murugan N (2006) Development of mathematical models for prediction of weld bead geometry in cladding by flux cored arc welding. Int J Adv Manuf Technol 30:669–676
16. Manonmani K, Murugan N, Buvanasekaran G (2007) Effects of process parameters on the bead geometry of laser beam butt welded stainless steel sheets. Int J Adv Manuf Technol 32:1125–1133
17. Khan MMA, Romoli L, Fiaschi M, Dini G, Sarri F (2012) Multi-response optimization of laser welding of stainless steels in a constrained fillet joint configuration using RSM. Int J Adv Manuf Technol 62:587–603
18. Badkar DS, Pandey KS, Buvanashekaran G (2012) Application of the central composite design in optimization of laser transformation hardening parameters of commercially pure titanium using Nd:YAG laser. Int J Adv Manuf Technol 59:169–192
19. Onwubolu GC, Davim JP, Oliveira C, Cardoso A (2007) Prediction of clad angle in laser cladding by powder using response surface methodology and scatter search. Opt Las Technol 39:1130–1134
20. Mondal S, Bandyopadhyay A, Pal PK (2011) Ni-Cr-Mo cladding on mild steel surface using CO2 laser and process modeling with response surface methodology (RSM). Int J Eng Sci Technol 3(8): 6805–6816
21. Sun Y, Hao M (2012) Statistical analysis and optimization of process parameters in Ti6Al4V laser cladding using Nd: YAG laser. Opt Las Eng 50:985–995
22. Wu CFJ, Hamada M (2009) Experiments: planning, analysis, and optimization (2nd Edition), Wiley.
23. Li YY, Liu JC (2010) Effects of the gas flow and the defocusing distance from laser beam focus on powder feed laser cladding. In: Proc of SPIE, 7843.
24. Derringer G, Suich R (1980) Simultaneous optimization of several response variables. J Qual Technol 12(4):214–219
25. Washko JF, Parker HK, Brookshier SW (2012) Powder-delivery apparatus for laser-cladding, Patent Application: US 2012/0199564 A1.